Influence of the initial angular distribution on strong-field molecular dissociation

Youliang Yu, Shuo Zeng, J. V. Hernández, Yujun Wang, and B. D. Esry

J. R. Macdonald Laboratory, Kansas State University, Manhattan, Kansas 66506, USA

We study few-cycle, strong-field dissociation of aligned H_2^+ by solving the time-dependent Schrödinger equation including rotation. We examine the dependence of the final angular distribution, the kinetic energy release spectrum, and the total dissociation yield on the initial nuclear angular distribution. In particular, we look at the dependence on the relative angle θ_0 between the laser polarization and the symmetry axis of a well-aligned initial distribution, as well as the dependence on the delay between the "pump" pulse that prepares the alignment and the few-cycle probe pulse. Surprisingly, we find the dissociation probability for $\theta_0 = 90°$ can be appreciable even though the transitions involved are purely parallel. We therefore address the limits of the commonly held "ball-and-stick" picture for molecules in intense fields as well as the validity of the axial recoil approximation.

I. INTRODUCTION

Despite significant current interest in strong-field processes for initially well-aligned molecules, theoretical treatments that include the full nuclear dynamics, including rotation, for this problem have essentially not been pursued. Instead, the argument is usually made that rotation is slow compared to the electronic and vibrational dynamics as well as to the laser pulse and can thus be excluded from calculations [1]. It has been shown, though, that neglecting nuclear rotation can qualitatively change the dynamics; vibrational trapping, for example, is strongly suppressed by rotation, essentially eliminating it [2–4].

When rotation is neglected—but the angular distribution is desired—it is often obtained using the axial recoil approximation whereby the nuclei are assumed to dissociate along the same line they were held to during the pulse. Recent work [5], however, shows that this simple approach is insufficient for accurately describing the angular distribution of the nuclei following strong-field dissociation of H_2^+—even in an ultrashort pulse. This result can be understood [5] as impulsive alignment [6,7] of the dissociating fragments. That is, the ultrashort pulse produces a broad distribution of angular momenta that leads to substantial evolution of the angular distribution after the pulse. The axial recoil approximation is thus insufficient in these cases. However, Ref. [5] assumed an isotropic initial distribution of the molecule. What happens if the molecule is instead initially well aligned? Is the axial recoil approximation better in this case? Is the dissociation larger for an aligned molecule?

In this article, we begin to answer these questions by studying the influence of the initial angular distribution on H_2^+ dissociation in intense, few-cycle pulses. We imagine a pump-probe scheme in which the pump pulse—linearly polarized at an angle, θ_0, relative to the probe pulse—produces a well-aligned distribution at time t_i and the linearly polarized probe pulse dissociates the molecule after a delay, Δt. The initial angular distribution is thus characterized by its alignment angle θ_0 and its width.

We study the dependence of the angular distribution, the kinetic energy release (KER) spectrum, and the total dissociation yield on θ_0 and the initial angular width. We also investigate the Δt dependence of these dissociation observables. Among other things, we have found the surprising result that the

dissociation probability for perpendicular alignment can be appreciable even though the transitions involved are purely parallel.

II. THEORY

A. Time-dependent Schrödinger equation

The time-dependent Schrödinger equation (TDSE) for three-dimensional H_2^+ is written as

$$i\frac{\partial}{\partial t}\Psi(\boldsymbol{R},\boldsymbol{r},t) = [H_0 - \boldsymbol{d}\cdot\boldsymbol{\mathcal{E}}(t)]\Psi(\boldsymbol{R},\boldsymbol{r},t), \tag{1}$$

with field-free Hamiltonian H_0 and nuclear and electronic coordinates $\boldsymbol{R}$ and $\boldsymbol{r}$. Atomic units are used throughout this work unless otherwise noted. We use the dipole approximation in the length gauge with dipole operator $\boldsymbol{d}$. The probe electric field $\boldsymbol{\mathcal{E}}(t)$ is explicitly expressed as [8]

$$\boldsymbol{\mathcal{E}}_{\text{prob}}(t) = \hat{z}\mathcal{E}_0 e^{-t^2/\tau^2}\cos(\omega t + \varphi). \tag{2}$$

We use pulses with a full width of the intensity at half maximum, $\tau_{\text{FWHM}} = \tau\sqrt{2\ln 2}$, of 10 fs and a wavelength of 790 nm. The intensity is taken as 1.5×10^{13} W/cm^2 throughout the paper except where specified otherwise. Carrier-envelope phase effects are minimal for these pulse parameters [9], so we set $\varphi = 0$ for simplicity.

We solve Eq. (1) in the Born-Oppenheimer (BO) representation. The details of our method can be found in Refs. [4,10]. Here we provide a brief summary for completeness. First, the BO potentials and dipole matrix elements are calculated using the formulation in Ref. [10]. Then, the total wave function $\Psi(\boldsymbol{R},\boldsymbol{r},t)$ is expanded on the BO basis, and the nuclear rotation is treated via an expansion over symmetrized Wigner D functions. For our pulse parameters, retaining only the $1s\sigma_g$ and $2p\sigma_u$ channels is a good approximation [4]. In this case, both the Coriolis and non-Born-Oppenheimer couplings are zero. Equation (1) thus reduces to the coupled radial equation

$$i\frac{\partial}{\partial t}F_\alpha = \left(-\frac{1}{2\mu}\frac{\partial^2}{\partial R^2} + \frac{J(J+1)}{2\mu R^2} + U_\beta\right)F_\alpha$$
$$-\boldsymbol{\mathcal{E}}\cdot\sum_{\alpha'}\boldsymbol{D}_{\alpha\alpha'}F_{\alpha'}, \tag{3}$$

where $F_\alpha = F_\alpha(R,t)$ is the nuclear radial wave function. The index α collectively represent the quantum numbers βJM, with J and M the total orbital angular momentum and its laboratory-frame z projection, respectively, and β the electronic state label. In this work, $\beta = 1s\sigma_g$ and $2p\sigma_u$—or simply g and u. Consequently, only parallel transitions are allowed. The precise form of the dipole matrix element $\boldsymbol{D}_{\alpha\alpha'}$ is given in Ref. [4].

To solve Eq. (3), we use a generalized finite difference scheme for the radial coordinate [11–13] and split operator techniques combined with the Crank-Nicolson method for the time evolution, as implemented in Refs. [4,13,14]. We use a uniform radial grid distribution with 3000 points in the range 0.05 a.u. $\leqslant R \leqslant 80$ a.u. Time evolution starts at $t_{\min}$ when the pulse envelope first reaches 10^8 W/cm^2 and ends at t_f when it reaches 10^6 W/cm^2, with a time step of 0.5 a.u. All the results shown in this paper are tested to be converged to at least two digits.

B. Preparing the initial state

To study the effects of the initial angular alignment on strong-field molecular dissociation, we must prepare an appropriately aligned initial state. Instead of using an actual pump pulse for this purpose in our calculations, we directly construct the desired aligned state by superposing different JM states at time t_i. Due to the linearity of the TDSE, these states can be propagated independently and the results superposed as dictated by the initial state. In this section, we discuss the details of this procedure.

As shown in Fig. 1, our goal is to construct a state aligned along a line defined by the angles θ_0 and ϕ_0 with respect to the probe-pulse polarization, which also defines the quantization axis. Because the probe is linearly polarized, the choice of ϕ_0 is arbitrary—the results for any ϕ_0 can be obtained from another by a simple rotation about the z axis.

As the first step, we create a state aligned along z:

$$\Psi_{\text{aligned}} = \sum_{vJ} a_{vJ} \Phi_{JM}^v, \quad (4)$$

where $\Phi_{JM}^v = \chi_{vJ}\Omega_{M0}^{J\Pi}$, with χ_{vJ} the bound rovibrational radial eigenstate in the $1s\sigma_g$ channel and $\Omega_{M0}^{J\Pi}$ the symmetrized total orbital angular momentum state [4], with
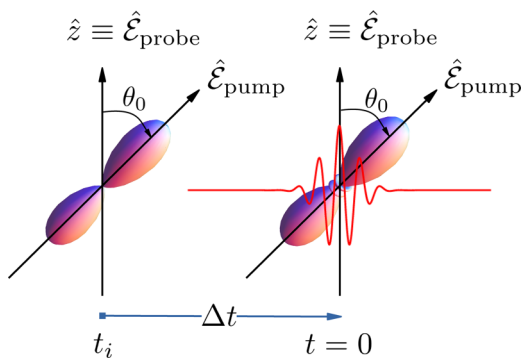

$$\hat{z} \equiv \hat{\mathcal{E}}_{\text{probe}} \qquad \hat{z} \equiv \hat{\mathcal{E}}_{\text{probe}}$$

FIG. 1. Schematic representation of the pump-probe scheme considered. The pump pulse creates a distribution at t_i aligned along $\hat{\mathcal{E}}_{\text{pump}}$. After a delay Δt, a probe pulse polarized at the angle θ_0 to the pump pulse dissociates the molecule.

Π the total parity. Without loss of generality, we assume $\Psi_{\text{aligned}} \sim \cos^n \theta$; therefore the coefficients a_{vJ} are defined by projecting $\cos^n \theta$ with $n = 6$ and 8 onto the eigenstates and normalizing the result. By choosing n even, only even Js (up to $J = 6$ or 8) contribute to Eq. (4), mimicking the production of Ψ_{aligned} by an impulsive pump pulse [6,7]. The phase of a_{vJ}, however, does not necessarily match that produced by impulsive alignment. The lack of R dependence in our target distribution primarily serves to enforce a phase convention on our numerically calculated $\chi_{vJ}(R)$. To have appreciable dissociation, we limit the sum to $v = 9$. With these choices, $\langle \cos^2 \theta \rangle$ for Ψ_{aligned} is 0.81 and 0.89 for $n = 6$ and $n = 8$, respectively, which are the two initial angular widths discussed throughout this work.

In the second step, the aligned state is rotated to the final angles (θ_0,ϕ_0) in the laboratory frame:

$$\Psi(t_i) = \hat{R}(\phi_0,\theta_0,0)\Psi_{\text{aligned}} = \sum_{JM} a_{vJ} D_{M0}^J(\phi_0,\theta_0,0)\Phi_{JM}^v, \quad (5)$$

using the rotation operator $\hat{R}$. As mentioned above, the choice of ϕ_0 is arbitrary; we thus set it to zero. We note that the solutions F_α of the TDSE in Eq. (3) depend only on $|M|$. The $-M$ solutions are thus identical to the $+M$ solutions.

Finally, the aligned initial state is prepared by propagating it freely from t_i to the beginning of the probe pulse at $t_{\min}$. This interval depends on the pump-probe delay as depicted in Fig. 1. The free evolution from t_i to $t_{\min}$ is purely analytic.

C. Superposing final states

Because the time evolution operator $U(t_f,t_i)$ is linear, applying it to $\Psi(t_i)$ only requires knowledge of the action of $U(t_f,t_i)$ on the individual rovibrational initial states in Eq. (5). Practically, we obtain this knowledge by solving Eq. (3), but we can write it conveniently as

$$\Phi_{JM}^v(t_f) = U(t_f,t_i)\Phi_{JM}^v(t_i), \quad (6)$$

since M is conserved by the linearly polarized probe pulse. To be clear, we note that the labels on $\Phi_{JM}^v(t_f)$ refer to the initial state—$\Phi_{JM}^v(t_f)$ itself will include all partial waves and both electronic states due to the action of $U(t_f,t_i)$.

According to Eq. (5), the total final state is thus expressed as

$$\Psi(t_f) = U(t_f,t_i)\Psi(t_i) = \sum_{JM} a_{vJ} D_{M0}^J(0,\theta_0,0)\Phi_{JM}^v(t_f). \quad (7)$$

In this way, we can propagate each initial state independently and superpose them with, in principal, arbitrary coefficients afterwards, providing a very efficient means of examining many initial angular distributions. It has the additional benefit of making the dependence on θ_0 explicit and analytic, which could be potentially useful.

D. Analysis

The complete formalism we use for analyzing H$_2^+$ dissociation with rotation can be found in Ref. [15]. Here, we only provide the modifications necessary for the present problem. For dissociation to $p + $ H, where H is in the $1s$

state asymptotically, the relative momentum distribution of
fragments is

$$\frac{\partial^2 P}{\partial \theta_K \partial E} = \int_0^{2\pi} d\phi_K \left| \langle \Psi_{\boldsymbol{K},1s}^{(-)} | \Psi(t_f) \rangle \right|^2, \tag{8}$$

where $\Psi_{\boldsymbol{K},1s}^{(-)}$ is the energy-normalized scattering wave function
with outgoing plane-wave boundary conditions, and $\boldsymbol{K}$ is the
relative nuclear momentum pointing from H to p. Note that
the full momentum distribution depends on the azimuthal angle
ϕ_K. It is peaked at ϕ_0, and the discussion of ϕ_0 above applies
here. However, since we are concerned primarily with the
behavior relative to the laser polarization—i.e., θ_K and θ_0—we
integrate over ϕ_K for all the results shown in this work.

The angular distribution can be obtained from the momen-
tum distribution using

$$\frac{dP}{d\theta_K} = \int_0^{\infty} \frac{\partial^2 P}{\partial \theta_K \partial E} dE, \tag{9}$$

whereas the KER distribution is

$$\frac{dP}{dE} = \int_0^{\pi} \frac{\partial^2 P}{\partial \theta_K \partial E} \sin \theta_K d\theta_K. \tag{10}$$

In practice, these integrations were carried out numerically.

III. RESULTS AND DISCUSSION

In our pump-probe scheme, the molecule is aligned at
t_i. After a delay Δt, an infrared probe pulse stimulates the
dissociation. However, the rotational wave packet evolves
freely from t_i until the probe arrives and will thus exhibit
revivals or partial revivals [7,15]. One might therefore expect
the results to be sensitive to the pump-probe delay. We
address this question in Sec. III A using the total dissociation
probability, the angular distribution, and the KER spectrum
of dissociation fragments. We address the θ_0 and width
dependence in Secs. III B and III C, respectively.

A. Pump-probe delay dependence

In this section, we discuss the Δt dependence of dissocia-
tion for a well-aligned initial state ($\Psi_{\text{aligned}} \propto \cos^8 \theta$, giving a
width of 0.89) with θ_0 restricted to zero.

In Fig. 2(a), we show the delay dependence of the field-free
$\langle \cos^2 \theta \rangle$ at $t = 0$, the total dissociation yield P, and $\langle \cos^2 \theta_K \rangle$
for the dissociation fragments. The field-free $\langle \cos^2 \theta \rangle$ gives
the alignment at $t = 0$ with no probe pulse. And, as one might
expect, P follows the field-free $\langle \cos^2 \theta \rangle$—in other words, P
grows when $\langle \cos^2 \theta \rangle$ grows, indicating that the more aligned
the molecule is, the more it dissociates since only parallel
transitions are possible between $1s\sigma_g$ and $2p\sigma_u$. The alignment
of the dissociation fragments $\langle \cos^2 \theta_K \rangle$ generally also follows
$\langle \cos^2 \theta \rangle$, but is larger at all delays. This result is consistent
with the observation in Ref. [5] that a short pulse impulsively
aligns the dissociating fragments.

Figure 2(b) shows the fragments' alignment in detail via
$dP/d\theta_K \sin \theta_K$ as a function of Δt. One can see that at
$\Delta t \approx 270$ fs, for example, where Fig. 2(a) shows the molecule
is at a local maximum of the initial alignment, the final angular
distribution is localized near 0 and π. Similar localization
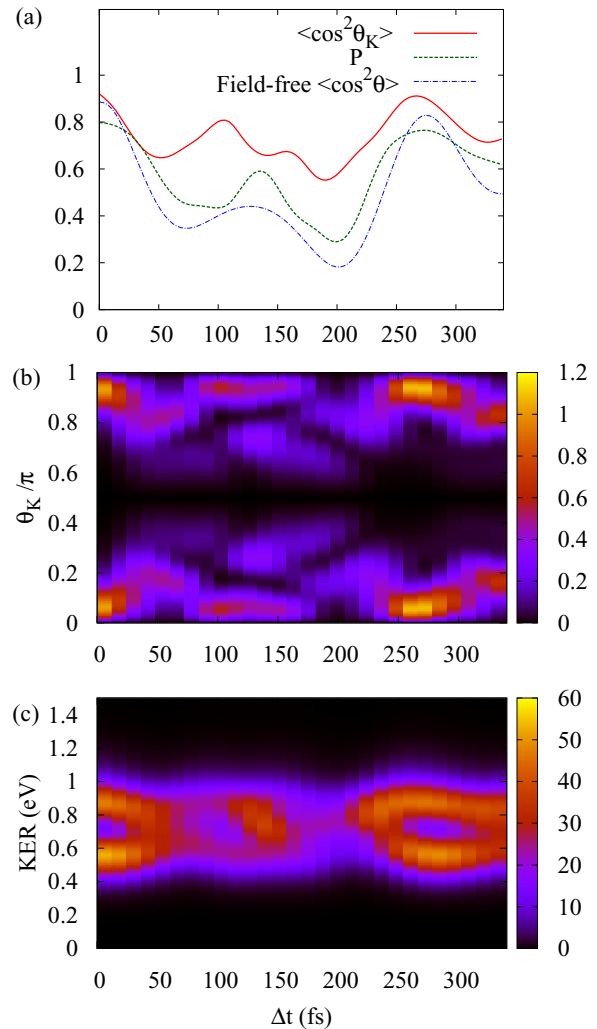occurs at $\Delta t = 0$ and $\Delta t \approx 130$ fs, where $\langle \cos^2 \theta \rangle$ peaks. In

FIG. 2. The pump-probe delay dependence of: (a) $\langle \cos^2 \theta_K \rangle$
(solid red line), the dissociation yield (dashed green line), and the
field-free $\langle \cos^2 \theta \rangle$ (dot-dashed blue line); (b) the angular distribution
$dP/d\theta_K \sin \theta_K$; and (c) the kinetic energy release spectrum.

contrast, when $\langle \cos^2 \theta \rangle$ is near a minimum—e.g., at $\Delta t \approx 70$,
200, and 350 fs—the peaks in the final angular distribution
move away from 0 and π, producing corresponding local min-
ima in $\langle \cos^2 \theta_K \rangle$. Since these minima in $\langle \cos^2 \theta \rangle$ correspond
to both aligned and antialigned initial distributions, the fact
that they all produce a minimum in $\langle \cos^2 \theta_K \rangle$ implies that
properties of the rovibrational wave packet beyond its width
are important. In particular, many different distributions—with
different phases—can have the same $\langle \cos^2 \theta \rangle$. It is natural that
the dynamics of these various wave packets differ. In fact,
Figs. 2(a) and 2(b) demonstrate this since different angular
distributions and yields result from initial states with the same
$\langle \cos^2 \theta \rangle$.

In Fig. 2(c), we show the delay-dependent KER spec-
trum for the dissociation fragments. For $v = 9$, one-photon
absorption should be dominant for the current laser param-
eters [1,4,16], which is consistent with Fig. 2(c) since the
position of the peak matches that expected for net one-photon
dissociation. An obvious feature of this plot is the oscillation
between the double-peaked structure and the single-peaked

structure. The double peak occurs near the delays with strong alignment, whereas the single peak happens at delays when $\langle \cos^2 \theta \rangle$ is near a minimum. We discuss such double-peaked KER more fully below.

B. Alignment angle dependence

Previous studies [17–21] indicate that molecular ionization and electron rescattering are sensitive to the molecule's alignment. In this section, we investigate the dependence of dissociation on the alignment angle. We again use a well-aligned initial state ($\propto \cos^8 \theta$), and the time delay is restricted to $\Delta t = 0$.

In Fig. 3(a), we show the total dissociation yields for two different intensities. For 1.5×10^{13} W/cm^2, we find that, for such a narrow initial angular distribution, there is a surprisingly large probability of dissociation at $\theta_0 = \pi/2$ compared with $\theta_0 = 0$, especially given that we do not include perpendicular transitions in the calculation. The simple no-rotation model employed by many for the nuclear dynamics would, of course, predict no dissociation for $\theta_0 = \pi/2$ at its simplest level of application. This suggests that the dissociation from such a narrow initial state must be due to its nonzero angular width. For comparison, we also show the result for 1.5×10^{11} W/cm^2. It can be seen that even for this much lower intensity, there is still appreciable dissociation for perpendicular alignment—about 11% of that for parallel alignment.

To help understand the dependence of dissociation on θ_0, we show in Fig. 3(b) the angular distribution of the fragments for 1.5×10^{13} W/cm^2 as a function of θ_0. At $\theta_0 \approx 0$, the dissociation probability peaks near $\theta_K = 0$ and $\theta_K = \pi$ as expected. As θ_0 becomes larger—but smaller than $\pi/4$—the peak of the angular distribution in θ_K approximately follows θ_0.

That is, $\theta_K \approx \theta_0$ and, by symmetry since we integrate over ϕ_0, $\theta_K \approx \pi - \theta_0$. This is the behavior one would expect according to the axial recoil approximation under the assumption that there is negligible change in the angular distribution during the pulse, which is probably a reasonable assumption for the 10-fs pulse used here. For θ_0 larger than about $\pi/4$, however, the peak in θ_K is no longer approximately θ_0. In this case, the assumption that the molecule does not rotate during the pulse implies that the axial recoil approximation at its simplest level is failing.

As suggested above, the axial recoil approximation might be salvaged by taking into account the finite angular width of the initial state rather than imagining it as a δ function at θ_0. For concreteness, let us consider the limiting $\theta_0 = \pi/2$ case with the simplified initial angular distribution $|\Psi|^2 \propto \cos^{16}(\theta - \pi/2)$ with a FWHM of just under 0.2π. In the axial recoil approximation, the θ_K distribution in Fig. 3(b) must originate from the wings of the initial distribution since there should still be no rotation during the pulse. However, if one calculates the probability that the molecule initially lies in the wings—i.e., $0 \leqslant \theta \leqslant 0.4\pi$ or $0.6\pi \leqslant \theta \leqslant \pi$—it turns out to be 18%, capturing only 60% of the dissociation shown in Fig. 3(a) for $\theta_0 = \pi/2$. Using this reasoning, one must therefore have dissociation originating from θ closer to $\pi/2$, which means, in turn, that these fragments must rotate after the pulse to give the distribution in Fig. 3(b). The bottom line is that the axial recoil approximation breaks down. Thus, while a nonzero initial angular width is required for dissociation at larger θ_0, rotational dynamics are also required to explain the final result.

We note that the common no-rotation treatment would predict a distribution superficially resembling Fig. 3(b) through the use of an effective intensity [7], $I_{\text{eff}} = I_0 \cos^2 \theta_0$ (the intensity due to the component of the laser field along the molecular axis). For a one-photon transition, this approach would predict an angular distribution immediately after the pulse proportional to $\cos^{16}(\theta - \pi/2) \cos^2 \theta$ for $\theta_0 = \pi/2$. This distribution peaks at $\theta = 0.4\pi$ and 0.6π. Post-pulse rotation would thus still be required to obtain the observed distribution. Considering three-photon transitions—i.e., $\cos^{16}(\theta - \pi/2) \cos^6 \theta$—moves the peaks less than 0.1π, still leaving the peak $\sim 0.05\pi$ short of the result in Fig. 3(b). All evidence thus points to the importance of rotation—and the breakdown of the axial recoil approximation—for quantitatively predicting the final angular distribution.

Figure 4 shows the KER distribution as a function of θ_0. The most striking feature is probably the transition from a single peak to a double peak much like in Fig. 2(c). The overall position of the peaks matches that for net-one-photon dissociation of $v = 9$ as expected. To understand the KER dependence, consider that the energy dependence of a purely one-photon dissociation peak is given in first-order perturbation theory by the pulse's power spectrum, the energy dependence of the dipole matrix element [15], and the spread in energy of the initial rovibrational states. In the present case, the pulse is Gaussian, giving a Gaussian power spectrum of width ≈ 0.2 eV; the dipole matrix element is smooth over this energy range with no zeros; and the initial states cover an energy range of about 0.19 eV. Thus, a one-photon transition cannot give two KER
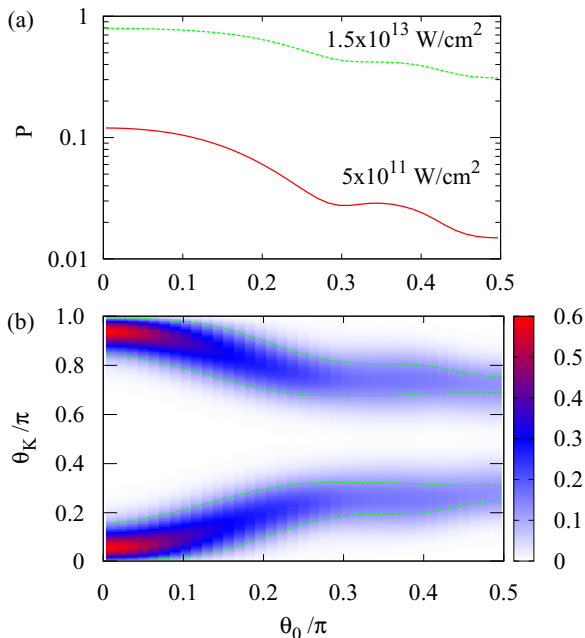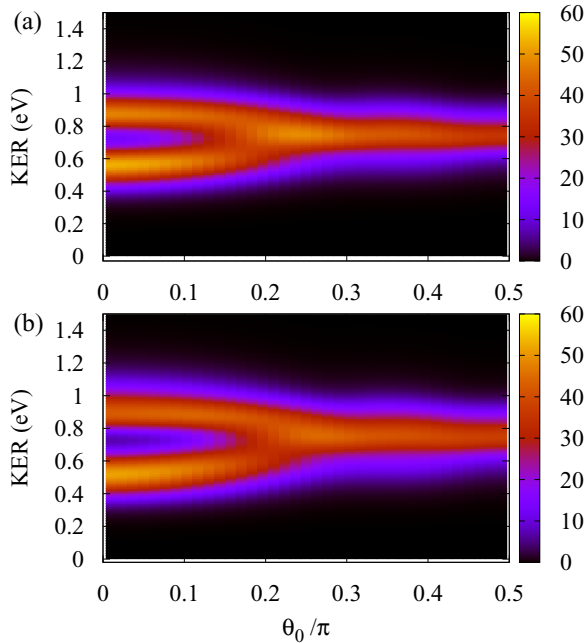

FIG. 3. The alignment angle (θ_0) dependence of: (a) the total dissociation probability, and (b) the angular distribution of the dissociation fragments $dP/d\theta_K \sin \theta_K$ for 1.5×10^{13} W/cm^2.

FIG. 4. Kinetic energy release spectrum of the dissociation fragments in terms of the alignment angle θ_0 for (a) 1.5×10^{13} W/cm^2 and (b) 2×10^{13} W/cm^2.

peaks in the present case—higher-order processes must be responsible. For instance, when three-photon processes—the next order that can contribute to the spectra in Fig. 4—become possible, then

$$\frac{dP}{dE} = \left| A_1 \mathcal{E}_0 + A_3 \mathcal{E}_0^3 \right|^2, \tag{11}$$

where A_i are the energy-dependent, complex, first- and third-order perturbation theory amplitudes. Only when $|A_3 \mathcal{E}_0^3| \approx |A_1 \mathcal{E}_0|$ can the nearly completely destructive interference required to produce two peaks occur. This observation can be used to understand Fig. 4.

Generally speaking, one would think to increase the three-photon contribution by increasing the intensity. However, the same result can be obtained by increasing the magnitude of the dipole matrix elements: A_1 is proportional to a dipole matrix element; and A_3, to a product of three dipole matrix elements. These dipole matrix elements depend on the quantum number M via the Clebsch-Gordan coefficients. With the M dependence analytic [4], it is straightforward to verify that the dipole matrix element decreases with increasing $|M|$. Further, the decrease can be roughly a factor of 2 from $M = 0$ to $|M| = J$, which is equivalent to reducing the intensity by a factor of 4. In an initial state with small θ_0, $M = 0$ dominates the distribution [see Eq. (5)], yielding a larger dipole matrix element. As θ_0 increases, larger $|M|$'s get populated, so the dipole matrix element is smaller and higher-order effects become negligible.

A more simplistic picture for understanding the emergence of the double-peaked spectrum can be found in the no-rotation model [1,22]. Specifically, with no rotation of the nuclei and only parallel transitions included, only the effective field $\mathcal{E}_{\text{eff}} = \mathcal{E}_0 \cos \theta_0$ enters the dipole interaction. This implies
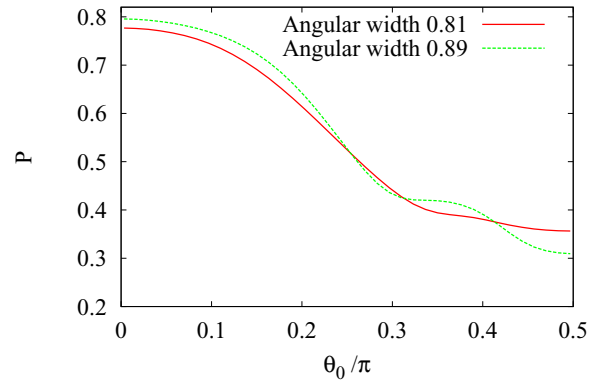

FIG. 5. Dissociation probability as a function of the alignment angle θ_0 for initial alignment widths 0.89 (dashed green line) and 0.81 (solid red line).

that the smaller θ_0 is, the greater $\mathcal{E}_{\text{eff}}$ is. Thus, higher-order processes become more probable as θ_0 decreases, permitting a double-peaked spectrum as described above. While this simple picture does qualitatively explain the figure and should apply so long as the molecule does not have time to rotate during the pulse [5], we have already detailed why including rotation after the pulse is essential for correctly predicting the final angular distribution.

C. Initial angular width

The previous sections have assumed an initial angular width of 0.89. Here, we address how the quality of the initial alignment affects the molecular dissociation. Specifically, we compare the θ_0 and the Δt dependence of dissociation for alignment widths of 0.89 and 0.81.

In Fig. 5, we show the θ_0 dependence of the total dissociation probability, repeating P for 0.89 from Fig. 3(a) for comparison. Overall, the trends are quite similar—parallel alignment leads to more dissociation than perpendicular alignment, as explained in the discussion of the θ_0 dependence in Sec. III B. Moreover, as θ_0 approaches zero, the narrower initial angular distribution gives a larger dissociation yield. This can be understood by noting that the dipole matrix elements also depend on the quantum number J via the Clebsch-Gordan coefficients. The initial J distribution is determined by the angular width in Eq. (4): the narrower the width, the broader the J distribution. Since the maximum populated J is larger, the dipole matrix elements are larger. The increase is about 15% from $J = 6$ to $J = 8$ given $M = 0$ for a parallel transition. Therefore, the narrower the angular distribution is, the more the molecule dissociates.

Finally, in Fig. 6 we compare the Δt dependence of the yield P and the field-free $\langle \cos^2 \theta \rangle$ (at $t = 0$) for different initial angular widths. As in Fig. 2(a) for the narrower initial angular distribution, the yields follow the same trend as the field-free $\langle \cos^2 \theta \rangle$. The yields for the different initial angular widths cross each other at approximately the same Δt as the field-free $\langle \cos^2 \theta \rangle$ equal each other for $\Delta t < 200$ fs. Such behavior, however, does not hold for larger Δt. This is simply because the details of the molecule's angular distribution might be different, even for the same $\langle \cos^2 \theta \rangle$.
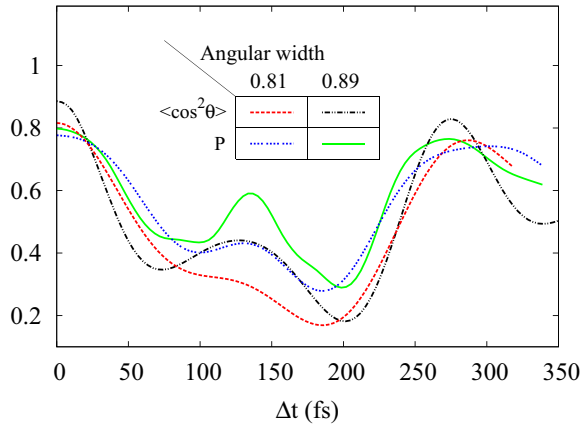
FIG. 6. Dissociation probability (dashed blue and solid green lines) and field-free $\langle \cos^2 \theta \rangle$ (dashed red and dot-dashed black lines) in terms of the time delay Δt for $\langle \cos^2 \theta \rangle = 0.89$ and $\langle \cos^2 \theta \rangle = 0.81$, both with $\theta_0 = 0$.

IV. SUMMARY

We have presented a study of the dependence of strong-field, few-cycle dissociation on the initial alignment of the molecule. We focused on H_2^+ and on initial distributions well aligned along an axis different from the polarization of the probe pulse. We have found evidence for post-pulse rotation—and thus the breakdown of the axial recoil approximation—especially when the angle between the alignment axis and probe polarization exceeds $45°$. Our calculations thus provide further evidence that the rotation of the nuclei must be included to quantitatively predict the momentum (or angular) distribution of strong-field dissociation. We have provided quantum-mechanical explanations of the observed phenomena, comparing and contrasting them with those based on simplified pictures commonly found in the literature. We expect these results to apply not just to H_2^+, but to any diatomic molecule dissociating via parallel transitions due to a laser pulse that is short compared to the free rotation period.

[1] A. Giusti-Suzor, F. H. Mies, L. F. DiMauro, E. Charron, and B. Yang, J. Phys. B **28**, 309 (1995).

[2] A. Giusti-Suzor and F. H. Mies, Phys. Rev. Lett. **68**, 3869 (1992).

[3] E. E. Aubanel, A. Conjusteau, and A. D. Bandrauk, Phys. Rev. A **48**, R4011 (1993).

[4] F. Anis and B. D. Esry, Phys. Rev. A **77**, 033416 (2008).

[5] F. Anis, T. Cackowski, and B. D. Esry, J. Phys. B **42**, 091001 (2009).

[6] F. Rosca-Pruna and M. J. J. Vrakking, Phys. Rev. Lett. **87**, 153902 (2001).

[7] H. Stapelfeldt and T. Seideman, Rev. Mod. Phys. **75**, 543 (2003).

[8] The laser electric field in atomic units is $\mathcal{E}_0 = \sqrt{I/I_{au}}$, where I is intensity in W/cm^2 and $I_{au} = 3.51 \times 10^{16}$ W/cm^2 is defined based on the proton's electric field in the first Bohr orbit, see App. 14, B. H. Bransden and C. J. Joachain, *Physics of Atoms and Molecules* (Prentice Hall, New York, 2003).

[9] F. Anis and B. D. Esry, Phys. Rev. Lett. **109**, 133001 (2012).

[10] B. D. Esry and H. R. Sadeghpour, Phys. Rev. A **60**, 3604 (1999).

[11] S. E. Koonin, K. T. R. Davies, V. Maruhn-Rezwani, H. Feldmeier, S. J. Krieger, and J. W. Negele, Phys. Rev. C **15**, 1359 (1977).

[12] J. Colgan, M. S. Pindzola, and F. Robicheaux, Phys. Rev. A **68**, 063413 (2003).

[13] M. W. J. Bromley and B. D. Esry, Phys. Rev. A **69**, 053620 (2004).

[14] F. Anis, V. Roudnev, R. Cabrera-Trujillo, and B. D. Esry, Phys. Rev. A **73**, 043414 (2006).

[15] F. Anis, Ph.D. thesis, Kansas State University, 2009.

[16] J. H. Posthumus, Rep. Prog. Phys. **67**, 623 (2004).

[17] E. Volkova, A. Popov, and O. Tikhonova, J. Exp. Theor. Phys. **97**, 702 (2003).

[18] T. K. Kjeldsen, L. B. Madsen, and J. P. Hansen, Phys. Rev. A **74**, 035402 (2006).

[19] H. Yu and A. D. Bandrauk, J. Chem. Phys. **102**, 1257 (1995).

[20] M. Lein, N. Hay, R. Velotta, J. P. Marangos, and P. L. Knight, Phys. Rev. A **66**, 023805 (2002).

[21] C. B. Madsen and L. B. Madsen, Phys. Rev. A **74**, 023403 (2006).

[22] P. Q. Wang, A. M. Sayler, K. D. Carnes, J. F. Xia, M. A. Smith, B. D. Esry, and I. Ben-Itzhak, Phys. Rev. A **74**, 043411 (2006).